Quantitative parameter analysis of pretreatment dual-energy computed tomography in nasopharyngeal carcinoma cervical lymph node characteristics and prediction of radiotherapy sensitivity

Zhiru Li[1,2,3†], Chao Li[4†], Liyan Li[5], Dong Yang[2,3], Shuangyue Wang[2,3], Junmei Song[2,3], Muliang Jiang[5*] and Min Kang[2,3*]

Abstract

Background Treatment efficacy may differ among patients with nasopharyngeal carcinoma (NPC) at similar tumor–node–metastasis stages. Moreover, end-of-treatment tumor regression is a reliable indicator of treatment sensitivity. This study aimed to investigate whether quantitative dual-energy computed tomography (DECT) parameters could predict sensitivity to neck–lymph node radiotherapy in patients with NPC.

Methods Overall, 388 lymph nodes were collected from 98 patients with NPC who underwent pretreatment DECT. The patients were divided into complete response (CR) and partial response (PR) groups. Clinical characteristics and quantitative DECT parameters were compared between the groups, and the optimal predictive ability of each parameter was determined using receiver operating characteristic (ROC) analysis. A nomogram prediction model was constructed and validated using univariate and binary logistic regression.

Results DECT parameters were higher in the CR group than in the PR group. The iodine concentration (IC), normalized IC, Mix-0.6, spectral Hounsfield unit curve slope, effective atomic number, and virtual monoenergetic images were significantly different between the groups. The area under the ROC curve of the DECT parameters was 0.73–0.77. Based on the binary logistic regression, a column chart was constructed using 10 predictive factors, including age, sex, N stage, maximum lymph node diameter, arterial phase NIC, venous phase NIC, λHU and spectral Hounsfield units at 70 keV. The area under the ROC curve value of the constructed model was 0.813, with a sensitivity and specificity of 85.6% and 81.3%, respectively.

†Zhiru Li and Chao Li contributed equally to this work.

*Correspondence:
Muliang Jiang
jmlgxmu@gmail.com
Min Kang
kangmin@gxmu.edu.cn

Full list of author information is available at the end of the article

Conclusion Quantitative DECT parameters could effectively predict the sensitivity of NPC to radiotherapy. Therefore, DECT parameters and NPC clinical features can be combined to construct a nomogram with high predictive power and used as a clinical analytical tool.

Keywords Dual-energy CT, Nasopharyngeal carcinoma, Lymph nodes, Radiotherapy sensitivity

Introduction

Nasopharyngeal carcinoma (NPC) is a common malignant tumor of the neck with a high incidence in Southeast Asia [1]. Early radiotherapy alone can successfully control tumors, whereas concurrent chemotherapy is recommended for locally advanced NPC. The 5-year overall survival (OS) rate is reportedly 85% [2–4]. Recurrence and/or metastasis are the main causes of treatment failure [5, 6]. The tumor–node–metastasis (TNM) staging system is a key factor determining the treatment regimen and prognosis of distant metastasis [7]. However, distant metastases differ significantly among patients with similar TNM stages [8], and N staging is not considered comprehensive or sufficiently accurate [9, 10].

As radiotherapy and chemotherapy are the main treatment for NPC rather than surgery, clinical examinations cannot be used to accurately evaluate pathological specimens of NPC lymph nodes. Magnetic resonance imaging (MRI) has been widely used to measure lymph node sizes because of its excellent ability to measure soft tissue components [11]. However, false-positive or -negative results often occur because large lymph nodes may be reactive, and small lymph nodes may also contain metastases [12–14]. Functional MRI techniques, such as diffusion-weighted imaging, have limited sensitivity (71.0–95.5%) and specificity (72.7–95.0%) in differentiating solid tumors [14, 15]. In addition to the MRI diagnostic criteria for retropharyngeal and cervical lymph node metastases in the international consensus guidelines [16], lymph nodes with high radiotherapy and chemotherapy sensitivity should be considered positive nodes. Understanding lymph node characteristics and improving the control of metastatic cervical lymph nodes are helpful for prolonging patient survival.

Dual-energy computed tomography (DECT) is an advanced CT scanning technology used to, in addition to the traditional single-energy CT scan, perform reconstruction and quantitative analysis, improve tumor visibility, delineate tumor boundaries, and determine critical structures in head and neck imaging [17]. Low-energy virtual monoenergetic images (VMIs) can be used to improve pathological lymph node visibility, similar to primary tumors [18]. Studies have reported different quantitative DECT parameters that can be used to describe lymph nodes, with significant differences observed in the quantitative parameters obtained from the spectral Hounsfield unit attenuation curve slope and iodine maps (iodine content) of lymph nodes [19]. These studies indicate that quantitative analysis helps identify lymph nodes with different pathological features.

Studies on the prediction of neck-lymph node radiotherapy sensitivity to NPC based on DECT quantitative parameters are lacking. Therefore, this study aimed to investigate whether quantitative DECT parameters can predict cervical-lymph node radiotherapy sensitivity to NPC, construct a nomogram by combining clinical and pathological factors with quantitative DECT parameters, evaluate the robustness of this new clinical predictive model, and provide new ideas for clinical diagnosis and treatment of NPC.

Materials and methods

Patient population

This study was performed in accordance with the tenets of the Declaration of Helsinki (revised in 2013) and was approved by the Medical Ethics Committee of the First Affiliated Hospital of Guangxi Medical University. All patients signed an informed consent form after receiving a detailed explanation of the research. Between September 2021 and December 2022, 98 patients newly diagnosed with nasopharyngeal carcinoma underwent pretreatment DECT. The study included patients (I) with pathologically confirmed NPC; (II) who had not received radiotherapy or chemotherapy before surgery; and (III) without a history of iodine allergy or hyperthyroidism symptoms. The exclusion criteria were as follows: (1) incomplete clinical data; (2) poor image quality that could not be qualitatively or quantitatively analyzed; and (3) a history of tuberculosis, other head and neck malignancies, or lymphoma.

All patients underwent pretreatment dual-energy DECT and MRI scans 1–3 days before treatment with radical intensity-modulated radiation therapy and concurrent±induction chemotherapy. Radiotherapy was administered according to Reports 83 of the International Commission on Radiation Units and Measurements (ICRU) and the expert consensus of the Radiation Treatment Oncology Organization Group (RTOG) 0225. GTVnx includes primary NPC foci and enlarged retropharyngeal lymph nodes, whereas GTVnd includes imaging and palpation findings of enlarged cervical lymph nodes. The high-risk clinical target volume (CTV1) was a 5–10-mm outward expansion of the GTVnx (or 2–3 mm if close to the brainstem or spinal cord) to cover the submicroscopic increase in the high-risk site and entire nasopharynx. The low-risk clinical target volume (CTV2)

was a 5–10-mm outward expansion of CTV1 to include the foramen lacerum, sphenoid sinus, clivus, oval foramen, parapharyngeal space, pterygoid fossae, posterior parts of the nasal cavity, pterygopalatine fossae, and the lymph node drainage area in the neck. Treatment doses included PTVnx and PTVRPN (68–74 Gy), PTVND (66–70 Gy), PTV1 (60–66 Gy), and PTV2 (50–56 Gy). Five fractions/week and a total of 30–33 fractions were administered. All chemotherapy regimens were platinum-based (80–100 mg/m^2) and administered once every 3 weeks, including radiotherapy alone, concurrent chemoradiotherapy (CCRT), and CCRT after induction chemotherapy. Clinical and pathological data, including age, sex, body mass index, TNM staging, comorbidities, Epstein–Barr virus (EBV) DNA levels, radiation and chemotherapy status, and lymph node characteristics, were collected.

Data acquisition and image reconstruction
All patients were scanned using a DECT scanner (SOMATOM Definition Flash CT; Siemens, Erlangen, Germany). Patients were placed on a scanning bed and instructed to avoid swallowing, and scanning was performed from the base of the skull to the sternoclavicular joint. Scanning parameters were: tube voltages, 80 kV and 140 kV (with simultaneous application of CARE Dose 4D); reference tube current, 320 mA; collimation, 128×0.6 mm; rotation speed, 0.5 s/r; and pitch, 0.6. A sinogram affirmative reconstruction (SAFIRE) technique was used for the reconstruction. The reconstruction layer thickness was 1.5 mm, and the space between layers was 1 mm. A high-pressure syringe (85 mL; Nemoto Kyorindo Co. Ltd., Tokyo, Japan) was used to inject the contrast agent iopamidol (iopamidol 300; Bracco, Milan, Italy) intravenously through the median elbow at 1–1.5 mL/kg body weight and 3 mL/s. The common carotid artery was selected as the detection point, and the threshold was set at 100 HU. The scan delay period for the arterial and venous phases was 25 s and 50 s, respectively.

DECT image analysis
The reconstructed DECT image data were postprocessed using a workstation (VB20A; Siemens), and energy spectrum curve characteristics were analyzed using the "Liver VNC," "Single Energy+," and "Rho/Z" functions. Under different single-energy conditions (40, 50, 60, 70, …, 120 keV) and the corresponding single-energy conditions, when the image contrast-to-noise ratio value was the highest, the region of interest (ROI) was selected from the largest lymph node of each patient, and the CT value was calculated. The ROI included as many solid parts as possible, and each lesion was measured thrice in a blinded manner by three deputy chief physicians with over 10 years of experience in CT diagnosis. The iodine

concentration (IC), effective atomic number(Z_{eff}), spectral Hounsfield units at 40–100 keV (10-keV intervals), linear blending images with a blending ratio of 0.6 (Mix-0.6), and electron cloud density (Rho) of each lesion were recorded. The normalized IC (NIC) was calculated as IC(lesion)/IC(Common Carotid artery), and the spectral Hounsfield unit curve slope (λhu) was calculated as λhu = (HU40 keV-HU70 keV)/30 keV.

Clinical evaluation
According to the Response Evaluation Criteria in Solid Tumors version 1.1 [20], responses were divided into complete response (CR; lesion disappearance), partial response (PR; at least 30% reduction in nodal diameter based on baseline diameter), stable response (<30% reduction in nodal diameter), and progression (>20% increase in nodal diameter). Lesion changes in completely and partially responsive patients were repeatedly confirmed. The patients were divided into CR and PR groups (partial response+stable response) according to therapeutic effects.

The TNM staging criteria for tumors were adopted in the 2017 International Alliance Against Cancer/American Joint Committee on Cancer (AJCC) 8th edition TNM staging standards [21]. The nodal division was determined according to the 2013 international consensus guidelines [16, 22]. Diagnostic MRI criteria for metastatic lymphadenopathy included [23] (1) the smallest lymph node diameter in the largest cross-sectional image is ≥10 mm; (2) lymph nodes of any size with central necrosis or a contrast-enhancing rimor exocapsular invasion; (3) lymph node grouping (presence of ≥3 contiguous and confluent lymph nodes, each with MID 8–10 mm); (4) the maximum transverse diameter of retropharyngeal lymph node is ≥5 mm. All included lymph nodes were positive according to MRI diagnostic criteria.

According to the lymph node location, patients were further divided into groups based on regions bounded by the hyoid body and the lower margin of cricoid cartilage: the upper cervical lymph node group (UNP), in which the lymph nodes were located in the retropharyngeal, I, and II regions; the middle cervical lymph node group (MNP), in which the lymph nodes were located in the upper part of the III, VA, and above VI regions; and the lower cervical lymph node group (LNP), where positive lymph nodes were located in the IV, superior clavicular fossa, and inferior portions of the VB and subarea VI regions.

Statistical analysis
SPSS 26.0 (IBM Corp.) software was used for statistical analysis. Count data are expressed as percentages (%), and groups were compared using the χ^2 test. Measurement data are expressed as mean±standard deviation (x±s), and the groups were compared using an

Li *et al. Radiation Oncology*   (2024) 19:81

Page 4 of 11

Table 1 Baseline characteristics of patients with nasopharyngeal carcinoma

Characteristics	Number	%
Total	98	100
Age (years)		
≤45	43	43.9
>45	56	57.1
Sex		
Male	73	74.5
Female	25	25.5
BMI(kg/m^2)		
≤22.5	49	50
>22.5	49	50
AJCC stage		
II	2	2
III	23	23.5
IV	73	74.5
T stage		
T2	14	14.2
T3	37	37.8
T4	48	49
N stage		
N1	30	30.7
N2	22	22.4
N3	46	46.9
M stage		
M0	87	88.8
M1	11	11.2
Induction chemotherapy		
No	16	16.3
TP	43	43.9
GP	38	38.8
EBV DNA(copy/ml)		
≤2000	65	66.3
>2000	33	33.7

Table 2 Differences in lymph node response characteristics after radiotherapy

Characteristics	Total [n]	CR group [n]	PR group [n]	P value
Total	388	285	103	
Age (years)				
≤45	162	104	58	0.002
>45	226	181	45	
Sex				
Male	319	248	71	<0.001
Female	69	37	32	
BMI(kg/m2)				
≤22.5	183	127	56	0.232
>22.5	205	158	47	
AJCC stage				
II				
III	60	38	22	0.155
IV	328	247	81	
T stage				
T2	47	36	11	0.663
T3	167	116	51	
T4	174	133	41	
N stage				
N1	53	35	18	0.047
N2	49	33	16	
N3	286	217	69	
M stage				
M0	342	250	92	0.911
M1	46	35	11	
Induction chemotherapy				
No	34	19	15	0.239
TP	164	116	48	
GP	190	150	40	
EBV(copy/ml)				
≤2000	203	139	64	0.047
>2000	185	146	39	

independent sample t-test/Mann–Whitney U-test (depending on the normality of the data distribution). Intra- and interobserver agreements were assessed using intragroup correlation coefficients in relation to quantitative parameters. Logistic regression analysis was used to fit the significant parameters. Receiver operating characteristic (ROC) analysis was used to calculate the area under the ROC curve (AUC) to evaluate the diagnostic value of the quantitative DECT parameters for radiotherapy sensitivity. The cutoff value was determined using the maximum Youden index, and the sensitivity, specificity, and AUC were calculated according to the optimal cutoff value. Logistic regression analysis was used to fit the significant parameters of single factors, and independent prognostic factors were determined to construct a nomogram, decision curve, and calibration plot for model evaluation. The open-source statistical environments R (version 4.3.0, available at www.r-project.org) and the "rms", "foreign", "rio" and "roc" packages were used for statistical analysis. The threshold for statistical significance was set at $p < 0.05$.

Results

Participants and lymph node characteristics

Overall, 98 patients, comprising 73 men and 25 women aged 30–70 years (mean age: 46.9±10.9 years) with 388 lymph nodes, were included (Table 1). After radiotherapy, 285 and 103 lymph nodes were assigned to the CR and PR groups, respectively. The two groups differed significantly with respect to age, N stage, EBV DNA level, lymph node location, longest dimension (LD) and shortest dimension (SD) of lymph nodes, and MRI classification. However, no significant differences were observed with respect to sex; body mass index; the T, M or AJCC stage; or induction chemotherapy (Tables 2 and 3).

Table 3 Morphological characteristics of the nasopharyngeal carcinoma lymph nodes

Characteristics	Total	CR group	PR group	P value
	[n(%)]	[n(%)]	[n(%)]	
Total	388	285	103	
Lymph node location				
UNP	300	209	91	0.037
MNP	56	47	9	
LNP	32	29	3	
LD(cm)				
>1.5	143	92	51	0.023
$1 \geq D \leq 1.5$	164	125	39	
<1	81	68	13	
SD(cm)				
>1.5	128	83	45	0.043
$1 \geq D \leq 1.5$	179	134	45	
<1	81	68	13	

Table 4 Comparison of lymph node dual-energy computed tomography-derived quantitative parameters between the complete and partial response groups

DECT parameters	CR group	PR group	P value
Arterial phase			
IC(mg/mL)	1.82 ± 0.71	1.98 ± 0.61	0.035
NIC	0.15 ± 0.06	0.17 ± 0.05	0.039
Mix-0.6	76.94 ± 17.65	81.67 ± 14.28	0.007
λHU(HU/keV)	2.15 ± 0.79	2.36 ± 0.73	0.012
Z_{eff}	8.48 ± 0.34	8.58 ± 0.29	0.008
Rho	37.51 ± 6.65	38.54 ± 5.03	0.102
40 keV(HU)	183.78 ± 45.72	199.94 ± 40.23	0.007
50 keV (HU)	131.96 ± 32.02	142.67 ± 32.47	0.006
60 keV(HU)	100.55 ± 25.72	108.03 ± 22.23	0.006
70 keV(HU)	81.22 ± 18.94	86.81 ± 16.06	0.004
80 keV(HU)	68.51 ± 14.77	73.13 ± 12.21	0.002
90 keV(HU)	60.37 ± 11.91	64.01 ± 9.76	0.003
100 keV(HU)	54.74 ± 10.11	57.79 ± 8.19	0.003
Venous phase			
IC(mg/mL)	2.29 ± 0.56	2.45 ± 0.46	0.005
NIC	0.42 ± 0.09	0.45 ± 0.08	0.001
Mix-0.6	86.92 ± 16.08	92.11 ± 11.05	0.003
λHU(HU/keV)	2.72 ± 0.66	2.91 ± 0.51	0.004
Z_{eff}	8.72 ± 0.27	8.8 ± 0.21	0.003
Rho	38.63 ± 6.53	39.76 ± 5.17	0.077
40 keV(HU)	223.4 ± 46.07	237.31 ± 35.85	0.002
50 keV (HU)	157.61 ± 30.41	167.21 ± 23.73	0.001
60 keV(HU)	117.96 ± 20.95	124.76 ± 16.18	0.001
70 keV(HU)	93.85 ± 15.64	98.89 ± 12.06	0.001
80 keV(HU)	78.09 ± 12.22	81.95 ± 9.42	0.001
90 keV(HU)	67.55 ± 10.08	70.72 ± 7.68	0.001
100 keV(HU)	60.38 ± 8.75	63.01 ± 6.72	0.002

Comparison of quantitative DECT parameters

The quantitative DECT parameters in the CR group were higher than those in the PR group. The two groups differed significantly with respect to the arterial and venous phase IC, NIC, Mix-0.6, λHU, Z_{eff}, spectral Hounsfield units at 40–100 keV. Rho significantly differed between the arterial and venous phases (Table 4).

Relationship between lymph node characteristics and quantitative DECT parameters

Binary logistic regression analyses showed that age, sex, N stage, LD, arterial phase NIC, arterial phase λHU, arterial phase spectral Hounsfield units at 70 keV, venous phase NIC, venous phase IC, and venous phase Mix-0.6 were significantly associated with radiotherapy sensitivity (Fig. 1). Further analysis showed that all DECT parameters in the arterial phase, including IC, NIC, Mix-0.6, λHU, and Z_{eff}, were lower than those in the venous phase (Fig. 2). Subgroup analysis showed that there were significant differences in N stage, lymph node location, and LD among the parameter arterial phase IC, NIC, Mix-0.6, λHU, and Z_{eff}. N stage, LD, and SD showed significant differences in venous phase IC and λHU; lymph node location showed significant differences in venous phase IC, NIC, Mix-0.6, and λHU showed significant differences in venous phase IC, NIC, Mix-0.6, and λHU (Supplementary Fig. 1).

DECT parameters as predictors of therapeutic response

The cutoff values, AUC, accuracy, sensitivity, and specificity of the NIC, IC, Mix-0.6, λHU, Z_{eff}, and spectral Hounsfield units at 70 keV during the arterial and venous phases are presented in Table 5. The AUC of all DECT parameters ranged from 0.73 to 0.77 ($P < 0.001$). The best cutoff values for the arterial phase were 0.16, 2.05, 87.35, 2.36, 8.65, and 86.70, whereas those for the venous phase were 0.41, 2.25, 88.65, 2.92, 8.73, and 92.70.

Clinicopathological factors and DECT parameters were included in the univariate and multivariate logistic regression analyses, and DECT parameters with significant differences were classified as categorical variables based on the cutoff values. Finally, a nomogram based on 10 predictors, including age, sex, N stage, arterial phase NIC, arterial phase λHU, arterial phase spectral Hounsfield units at 70 keV, venous phase NIC, venous phase IC, and venous phase Mix-0.6 was constructed (Fig. 3). The AUC value of the nomogram was 0.84 (95% confidence interval: 0.81–0.88), with sensitivity and specificity of 85.66% and 81.3%, respectively, indicating that the AUC of the nomogram was superior to that of a single DECT parameter and that the model had good predictive ability (Fig. 4). Additionally, the calibration curve showed that the predictive ability of the nomogram model was highly consistent with actual radiotherapy sensitivity (Fig. 5). Decision curves of IC, NIC, and the nomogram revealed that the net benefits of the nomogram were higher than those of the DECT parameters (Fig. 5). All patients were divided into high- and low-risk group of
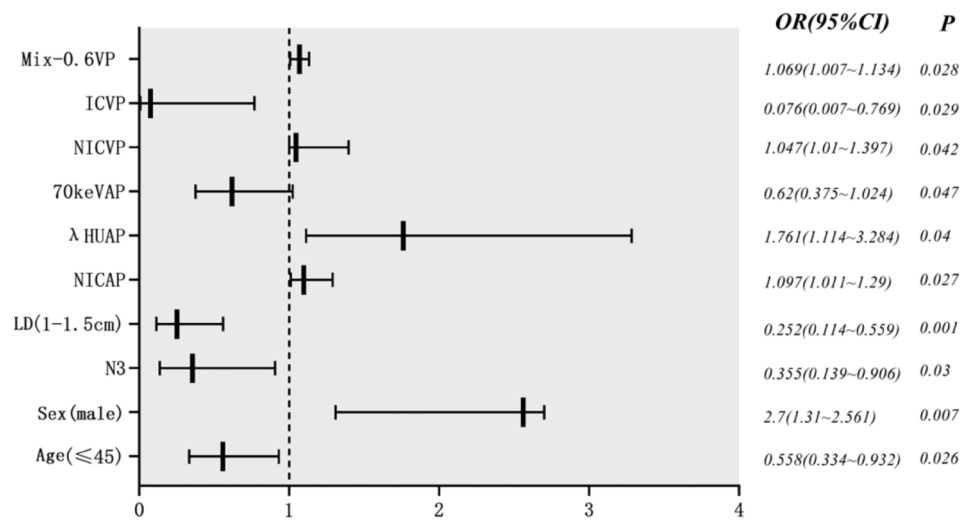
Li *et al. Radiation Oncology*   (2024) 19:81

Page 6 of 11

	OR(95%CI)	P
Mix-0.6VP	1.069(1.007~1.134)	0.028
ICVP	0.076(0.007~0.769)	0.029
NICVP	1.047(1.01~1.397)	0.042
70keVAP	0.62(0.375~1.024)	0.047
λHUAP	1.761(1.114~3.284)	0.04
NICAP	1.097(1.011~1.29)	0.027
LD(1-1.5cm)	0.252(0.114~0.559)	0.001
N3	0.355(0.139~0.906)	0.03
Sex(male)	2.7(1.31~2.561)	0.007
Age(≤45)	0.558(0.334~0.932)	0.026

Fig. 1 Multivariate analysis of clinical, pathological, morphological features and dual-energy parameters

LNM according to the optimal nomo-score cutoff value of -1.238 (corresponding to a total of 234 points in nomogram). The waterfall diagram displayed the distribution of nomo-scores and the status of lymph node sensitivity to radiotherapy (Fig. 6).

Discussion

Radiosensitivity is an important factor influencing the curative effects of NPC treatment. Gross tumor regression of primary tumors and/or metastatic lymph nodes at the end of intensity-modulated radiation therapy can be used to predict poor prognosis in patients with NPC [24, 25]. The difference in tissue radiosensitivity is the focus of research because of the significant differences in the clinical curative effect among patients receiving the same therapy and with similar EBV DNA levels, TNM stage, and pathological characteristics [26, 27].

Residual tumors appear after NPC radiotherapy, and tissue radiotherapy tolerance is related to several biological changes in the tumor and its microenvironment. The major factors are the degree of tissue hypoxia and the tumor molecular phenotype [26, 28, 29]. A close relationship exists between the blood supply and oxygen content of the tumor. The higher the blood supply and oxygen content, the higher the sensitivity to radiotherapy. The early prediction of radiosensitivity can lead to optimized treatment regimens and reduced medical costs. Conventional MRI often provides insufficient diagnostic evidence for the early prediction of the therapeutic efficacy of NPC treatment [30]. Recently, advanced MRI methods, including intravoxel incoherent motion diffusion-weighted, dynamic contrast-enhanced, and three-dimensional pseudo-continuous arterial spin labeling perfusion imaging, have been used to predict the therapeutic efficacy of NPC treatment [31, 32].

DECT can produce images of various substances (including mainly water, iodine, and calcium) separated into different material images, which can be quantitatively analyzed on different substrate images to obtain a tissue characteristic map that reflects the chemical composition of the tissue and quantifies the concentration of the component [33]. The distribution of IC in different tissues is reflected in the iodine characteristics of tumor angiogenesis [34–36]. Z_{eff} indicates the average atomic number of a mixture of composite substances in the tissue, which is related to the density of tumor cell components and tissue iodine content [37, 38]. Lower keV values can increase tumor visibility, whereas higher keV values can reduce beam hardening artifacts [39, 40]. λHU reflects the attenuation characteristics of the lesions under different energy conditions [41]. These DECT quantitative parameters can characterize tumor blood supply and reflect lymph node characteristics [36, 41–44].

To the best of our knowledge, this is the first study to use multiple quantitative DECT parameters to predict lymph node sensitivity to radiotherapy in patients with NPC. Our study showed that after radiotherapy, the DECT parameters of lymph node PR group were higher than those of CR group, and there were significant differences in IC, NIC, Mix-0.6,λHU, Zeff and spectral Hounsfield units at 40–100 keV in arterial and venous phases. It was suggested that lymph nodes in the PR group may have had higher blood vessel density. Multiple factors showed that arterial phase NIC, λHU, spectral Hounsfield units at 70 keV, venous phase NIC, IC, and Mix-0.6 were independent predictors.Some of the high-energy VMIs and Rho were not significantly different, consistent with the findings of Zhao et al. [41, 45, 46] but not with those of Liu et al. [47]. This may be due to differences
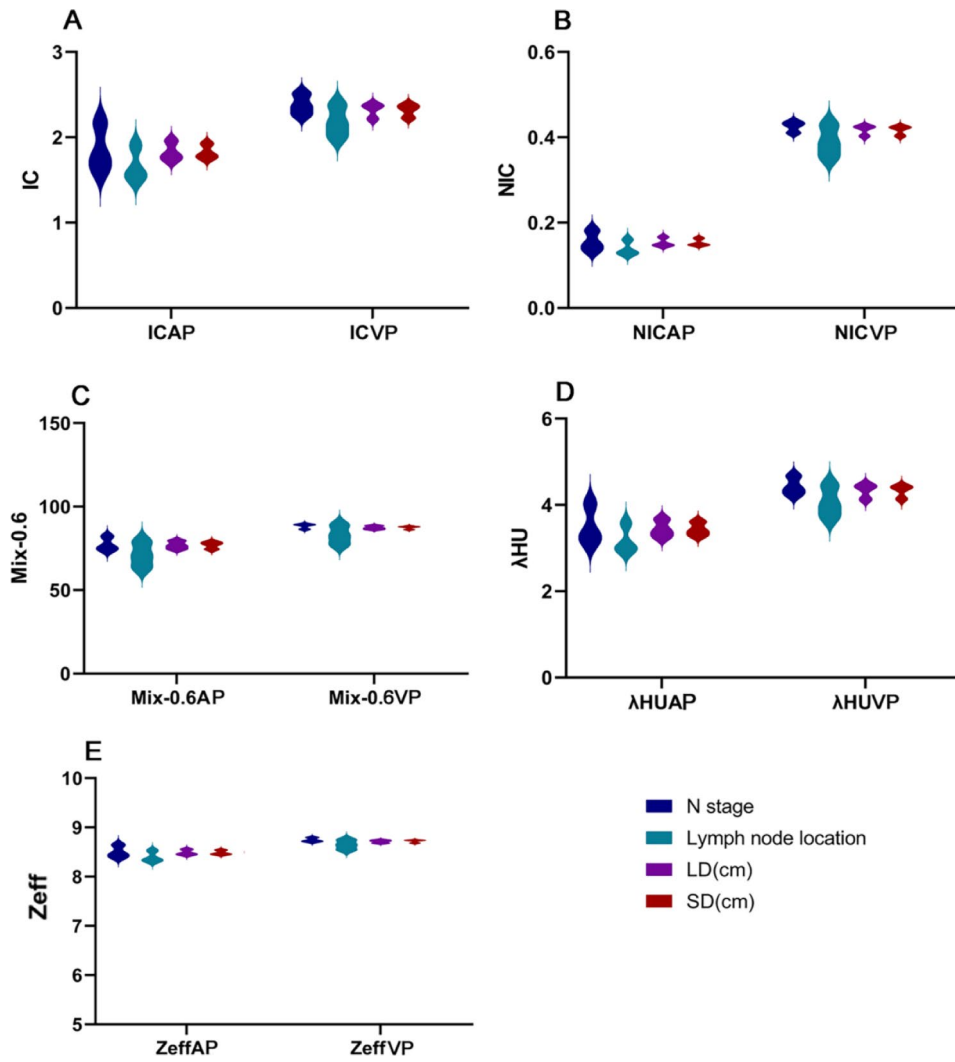
Fig. 2 Relationship between lymph node characteristics and dual-energy parameters. **A** Comparison of IC in arterial phase and venous phase of lymph node characteristics; **B** Comparison of NIC in arterial phase and venous phase of lymph node characteristics; **C** Comparison of Mix-0.6 in arterial phase and venous phase of lymph node characteristics; **D** Comparison of λhu in arterial phase and venous phase of lymph node characteristics; **E** Comparison of Zeff in arterial phase and venous phase of lymph node characteristics

Table 5 The value of arterial and venous dual-energy parameters (IC, NIC, Mix-0.6, λHU, Z_{eff}, and 70 keV) for radiotherapy sensitivity

	AUC	95%CI	Youden	Cutoff	Sensitivity	Specificity
Arterial phase						
NIC	0.73	(0.67–0.78)	0.34	0.16	0.64	0.70
IC	0.74	(0.68–0.79)	0.38	2.05	0.65	0.73
Mix-0.6	0.75	(0.69–0.79)	0.37	87.35	0.55	0.72
λHU	0.74	(0.68–0.79)	0.41	2.36	0.69	0.82
Zeff	0.74	(0.68–0.79)	0.37	8.65	0.60	0.77
70 keV	0.74	(0.69–0.79)	0.37	86.70	0.67	0.70
Venous phase						
NIC	0.73	(0.67–0.78)	0.40	0.41	0.86	0.64
IC	0.74	(0.69–0.79)	0.36	2.25	0.84	0.63
Mix-0.6	0.77	(0.72–0.82)	0.47	88.65	0.88	0.68
λHU	0.76	(0.71–0.81)	0.39	2.92	0.67	0.72
Zeff	0.75	(0.69–0.8)	0.37	8.73	0.83	0.65
70 keV	0.77	(0.72–0.81)	0.42	92.70	0.90	0.62
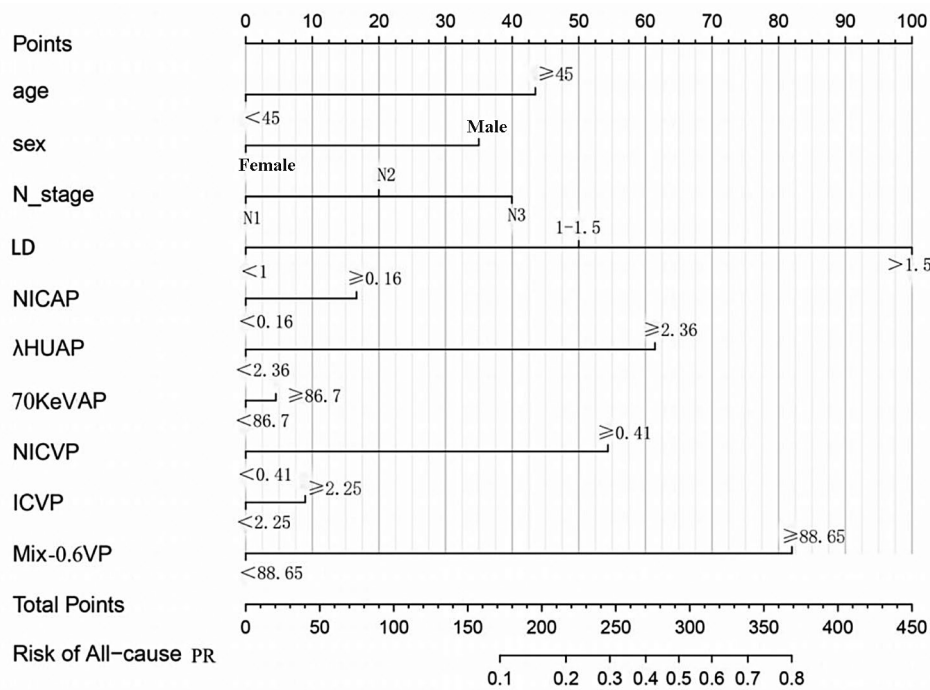
Fig. 3 Nomogram to predict radiotherapy sensitivity of nasopharyngeal carcinoma
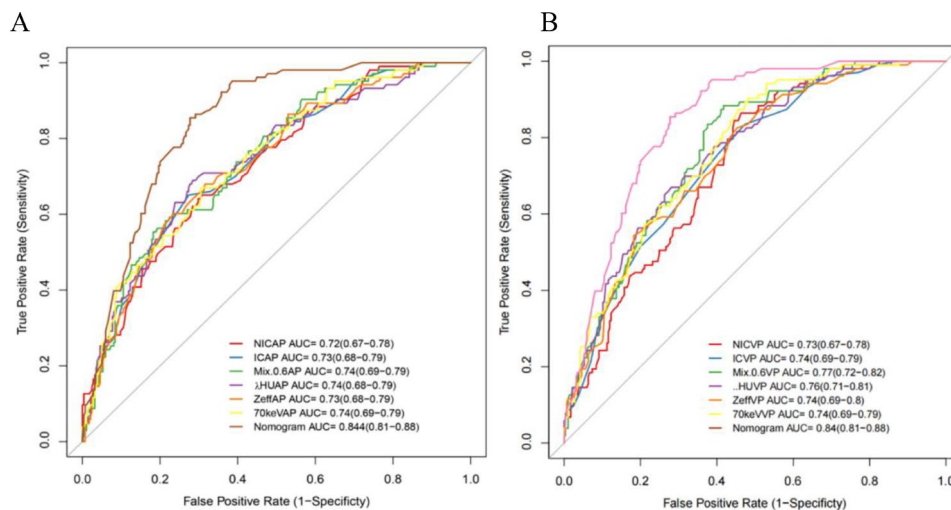
Fig. 4 Receiver operating characteristic curves of the nomogram and dual-energy parameters.(**A**) ROC curves of the nomogram and arterial phase dual-energy parameters; (**B**) ROC curves of the nomogram and venous phase dual-energy parameters

in the characteristics of the primary tumor and lymph nodes and the increased difference in iodine deficiency intensity of the high-energy VMIs. The heterogeneity of lymph nodes may be better reflected in low-energy VMIs and iodine maps.

Furthermore, we found that quantitative DECT parameters, such as IC, NIC, Mix-0.6, λHU, and Z_{eff}, were lower in the arterial phase than in the venous phase. The difference in iodine content parameters between the arterial and venous phases was greater, indicating a higher prediction, consistent with Qiu et al.'s study [46] on rectal

cancer lymph nodes. There were also differences in the arterial and venous phase parameters with different N stages, and lymph node locations and lengths, which we considered to be correlated with the degree of tumor invasiveness in patients with different clinical characteristics. For example, patients with high clinical stage tended to have large tumors with internal necrosis and loss of blood supply to the tumor stroma.

Using DECT to predict radiotherapy sensitivity in NPC, we found that the AUCs of IC, NIC, Mix-0.6, λHU, Z_{eff} and spectral Hounsfield units at 70 keV were

A

B
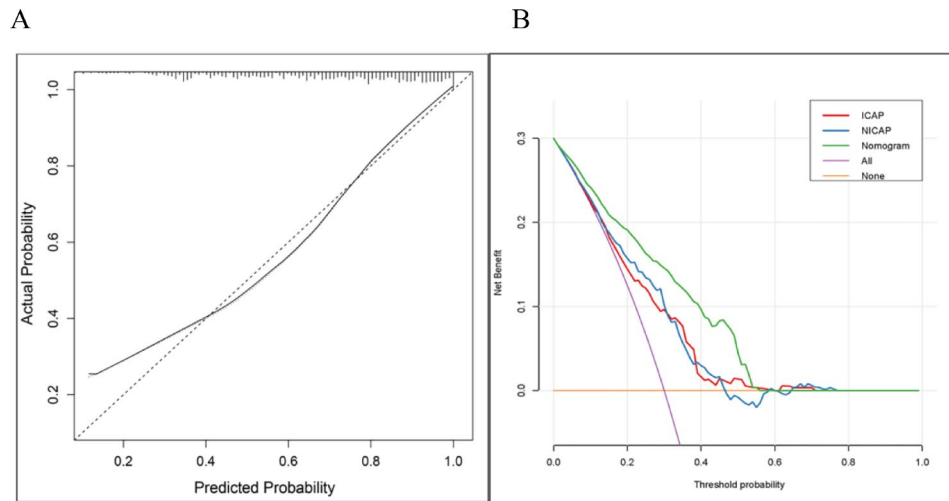
Fig. 5 Calibration curves and decision curves for the nomogram. (**A**) Calibration curves of the nomogram to predict radiotherapy sensitivity; (**B**) Decision curves for the nomogram and dual-energy parameters
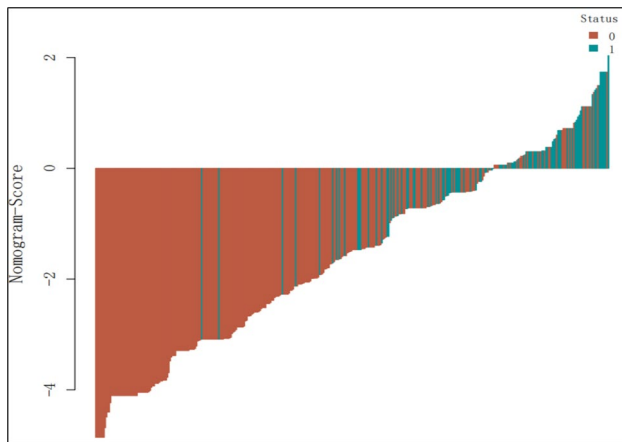

Fig. 6 Waterfall plot for distribution of Nomo-score in LNM prediction

equivalent (0.73–0.77) and slightly higher in the arterial phase than in the venous phase. Wang et al. [36] reported that DECT could simultaneously provide multiple parameters reflecting tumor parenchyma and vasculature information, which can minimize the overlap of DECT-derived single parameters and improve the overall performance of solid tumors in the differential diagnosis. In this study, univariate and multivariate regression analyses were performed to estimate clinicopathological variables and DECT parameters, and a nomogram containing 10 independent factors was established. The nomogram showed that LD, arterial λHU, venous NIC, and Mix-0.6 were more effective in establishing a predictive model with a higher AUC value (0.84), sensitivity and specificity were 85.6% and 81.3%, respectively, can be used to develop individualized treatment plans for patients with NPC, and is useful for the early identification of potential risks in radiotherapy-insensitive patients.

However, this study had some limitations. First, the ROI for measuring DECT-derived parameters did not fully reflect the overall characteristics of the lymph nodes. Second, this was a single-center study with no external validation such that DECT parameters may be subjected to contrast agents on a CT scanner, and the impact of differences in scanning and injection protocols and image artifacts in some patients was not validated. Third, we did not explore the correlation between primary tumors, histopathology features, and DECT parameters, which may also contribute to radiotherapy sensitivity prediction.

Conclusions

In this study, we demonstrated that patients with different nasopharyngeal carcinoma radiotherapy sensitivities have unique DECT imaging parameter characteristics that can be used to predict radiotherapy sensitivity. A visualized nomogram with combined clinical features was constructed, which is a new clinical analysis tool for predicting the radiosensitivity of patients with NPC.

Abbreviations

NPC	Nasopharyngeal Carcinoma
DECT	Dual-energy Computed Tomography
CR	Complete Remission
PR	Partial Remission
ROC	Receiver Operating Characteristic
IC	Iodine Concentration
AUC	LAS contraction
AF	Area Under the Curve
OS	Overall Survival
MRI	Magnetic Resonance Imaging
VMIs	Virtual Monoenergetic Images
CCRT	Concurrent Chemoradiotherapy
EBV	EpsteineBarr Virus
BMI	Body Mass Index
GP	Gemcitabine and Platinum
TP	Taxane and Platinum
UNP	Upper Neck Group
MNP	Middle Neck Group

LNP	Lower Neck Group
LD	The Longestdimension of Lymph Nodes
MRI	Magnetic Resonance Imaging
SD	The Shortest Dimension of Lymph Nodes
NIC	Normalized Iodine Concentration
Mix-0.6	Linear Blending Images with a Blending Ratio of 0.6
λHU	Slope of the sPectral Hounsfeld Unit Curve
Z_{eff}	Efective Atomic Number
Rho	Electron Cloud Density
AP	Arterial Phase
VP	Venous Phase
CI	Confdence Interval

Supplementary Information

The online version contains supplementary material available at https://doi.org/10.1186/s13014-024-02468-9.

Supplementary Material 1

Supplementary Material 2

Supplementary Material 5

Supplementary Material 6

Supplementary Material 7

Data availability
All data generated or analyzed during this study are included in this article and its supplementary information files.

Declarations

Ethics approval and consent to participate
This study was approved by the Ethics Committee of the First Affiliated Hospital of Guangxi Medical University (ethical approval number: 2023-E329-01).

Consent for publication
Not applicable.

Competing interests
The authors have no conflflicts of interest. All authors have read and approved the submitted manuscript. There are no conflflicts of interest. The manuscript has not been submitted elsewhere nor published elsewhere in whole or in part. All relevant ethical safeguards had been met. This study was approved by

our Institute Ethics Committee, and written informed consent was obtained from all patients.

Author details
[1]Department of Oncology, Sichuan Provincial People's Hospital·Qionglai Medical Center Hospital, Chengdu, Sichuan, People's Republic of China
[2]Department of Radiation Oncology, The First Affiliated Hospital of Guangxi Medical University, No. 6, Shuangyong Road, Nanning, Guangxi, Guangxi 530021, People's Republic of China
[3]Guangxi Tumor Radiation Therapy Clinical Medical Research Center, Nanning, Guangxi, People's Republic of China
[4]Department of Obstetrics and Gynecology, Sichuan Provincial People's Hospital·Qionglai Medical Center Hospital, Chengdu, Sichuan, People's Republic of China
[5]Department of Radiology, The First Affiliated Hospital of Guangxi Medical University, Nanning, Guangxi, People's Republic of China

References
1. Chen YP, Chan ATC, Le QT, Blanchard P, Sun Y, Ma J. Nasopharyngeal carcinoma. Lancet. 2019;394:64–80.
2. Blanchard P, Lee A, Marguet S, Leclercq J, Ng WT, Ma J, Chan AT, Huang PY, Benhamou E, et al. Chemotherapy and radiotherapy in nasopharyngeal carcinoma: an update of the MAC-NPC meta-analysis. Lancet Oncol. 2015;16:645–55.
3. Yang L, Hong S, Wang Y, Chen H, Liang S, Peng P, Chen Y. Development and External Validation of Nomograms for Predicting Survival in Nasopharyngeal Carcinoma patients after definitive Radiotherapy. Sci Rep. 2015;5:15638.
4. Hui EP, Ma BBY, Chan ATC. The emerging data on choice of optimal therapy for locally advanced nasopharyngeal carcinoma. Curr Opin Oncol. 2020;32:187–95.
5. Lee AW, Ma BB, Ng WT, Chan AT. Management of nasopharyngeal carcinoma: current practice and future perspective. J Clin Oncol. 2015;33:3356–64.
6. Xiao WW, Huang SM, Han F, Wu SX, Lu LX, Lin CG, Deng XW, Lu TX, Cui NJ, Zhao C. Local control, survival, and late toxicities of locally advanced nasopharyngeal carcinoma treated by simultaneous modulated accelerated radiotherapy combined with cisplatin concurrent chemotherapy: long-term results of a phase 2 study. Cancer. 2011;117:1874–83.
7. Zhang Y, Li WF, Mao YP, Zhou GQ, Peng H, Sun Y, Liu Q, Chen L, Ma J. Establishment of an integrated model incorporating standardised uptake value and N-classification for predicting metastasis in nasopharyngeal carcinoma. Oncotarget. 2016;7:13612–20.
8. Hui EP, Leung SF, Au JS, Zee B, Tung S, Chua D, Sze WM, Law CK, Leung TW, Chan AT. Lung metastasis alone in nasopharyngeal carcinoma: a relatively favorable prognostic group. A study by the Hong Kong Nasopharyngeal Carcinoma Study Group. Cancer. 2004;101:300–6.
9. Li JY, Huang CL, Luo WJ, Zhang Y, Tang LL, Peng H, Sun Y, Chen YP, Ma J. An integrated model of the gross tumor volume of cervical lymph nodes and pretreatment plasma Epstein-Barr virus DNA predicts survival of nasopharyngeal carcinoma in the intensity-modulated radiotherapy era: a big-data intelligence platform-based analysis. Ther Adv Med Oncol. 2019;11:1758835919877729.
10. Zhang J, Teng X, Lam S, Sun J, Cheung AL, Ng SC, Lee FK, Au KH, Yip CW et al. Quantitative spatial characterization of Lymph Node Tumor for N Stage improvement of nasopharyngeal carcinoma patients. Cancers (Basel) 15 (2022).
11. Chen J, Luo J, He X, Zhu C. Evaluation of contrast-enhanced computed tomography (CT) and magnetic resonance imaging (MRI) in the detection of Retropharyngeal Lymph Node Metastases in nasopharyngeal carcinoma patients. Cancer Manag Res. 2020;12:1733–9.
12. Guan Y, Liu S, Li AC, Pan XB, Liang ZG, Cheng WQ, Zhu XD. A pilot study: N-Staging Assessment of Shear Wave Elastrography in small cervical lymph nodes for nasopharyngeal carcinoma. Front Oncol. 2020;10:520.
13. Zhang GY, Liu LZ, Wei WH, Deng YM, Li YZ, Liu XW. Radiologic criteria of retropharyngeal lymph node metastasis in nasopharyngeal carcinoma treated with radiation therapy. Radiology. 2010;255:605–12.
14. Jin GQ, Yang J, Liu LD, Su DK, Wang DP, Zhao SF, Liao ZL. The diagnostic value of 1.5-T diffusion-weighted MR imaging in detecting 5 to 10 mm metastatic

cervical lymph nodes of nasopharyngeal carcinoma. Med (Baltim) 95, e4286 (2016).

15. Li H, Liu XW, Geng ZJ, Wang DL, Xie CM. Diffusion-weighted imaging to differentiate metastatic from non-metastatic retropharyngeal lymph nodes in nasopharyngeal carcinoma. Dentomaxillofac Radiol. 2015;44:20140126.

16. Lydiatt WM, Patel SG, O'Sullivan B, Brandwein MS, Ridge JA, Migliacci JC, Loomis AM, Shah JP. Head and Neck cancers-major changes in the American Joint Committee on cancer eighth edition cancer staging manual. CA Cancer J Clin. 2017;67:122–37.

17. Forghani R, Kelly HR, Curtin HD. Applications of dual-energy computed Tomography for the evaluation of Head and Neck squamous cell carcinoma. Neuroimaging Clin N Am. 2017;27:445–59.

18. Lam S, Gupta R, Levental M, Yu E, Curtin HD, Forghani R. Optimal virtual monochromatic images for evaluation of normal tissues and Head and Neck Cancer using dual-energy CT. AJNR Am J Neuroradiol. 2015;36:1518–24.

19. Forghani R. An update on advanced dual-energy CT for head and neck cancer imaging. Expert Rev Anticancer Ther. 2019;19:633–44.

20. Eisenhauer EA, Therasse P, Bogaerts J, Schwartz LH, Sargent D, Ford R, Dancey J, Arbuck S, Gwyther S, et al. New response evaluation criteria in solid tumours: revised RECIST guideline (version 1.1). Eur J Cancer. 2009;45:228–47.

21. Bossi P, Chan AT, Licitra L, Trama A, Orlandi E, Hui EP, Halamkova J, Mattheis S, Baujat B, et al. Nasopharyngeal carcinoma: ESMO-EURACAN clinical practice guidelines for diagnosis, treatment and follow-up(dagger). Ann Oncol. 2021;32:452–65.

22. Gregoire V, Ang K, Budach W, Grau C, Hamoir M, Langendijk JA, Lee A, Le QT, Maingon P, et al. Delineation of the neck node levels for head and neck tumors: a 2013 update. DAHANCA, EORTC, HKNPCSG, NCIC CTG, NCRI, RTOG, TROG consensus guidelines. Radiother Oncol. 2014;110:172–81.

23. Mao YP, Liang SB, Liu LZ, Chen Y, Sun Y, Tang LL, Tian L, Lin AH, Liu MZ, et al. The N staging system in nasopharyngeal carcinoma with radiation therapy oncology group guidelines for lymph node levels based on magnetic resonance imaging. Clin Cancer Res. 2008;14:7497–503.

24. Liang SB, Chen LS, Yang XL, Chen DM, Wang DH, Cui CY, Xie CB, Liu LZ, Xu XY. Influence of tumor necrosis on treatment sensitivity and long-term survival in nasopharyngeal carcinoma. Radiother Oncol. 2021;155:219–25.

25. Liang SB, Zhang N, Chen DM, Yang XL, Chen BH, Zhao H, Lu RL, Chen Y, Fu LW. Prognostic value of gross tumor regression and plasma Epstein Barr Virus DNA levels at the end of intensity-modulated radiation therapy in patients with nasopharyngeal carcinoma. Radiother Oncol. 2019;132:223–9.

26. Zhang Y, Zhang ZC, Li WF, Liu X, Liu Q, Ma J. Prognosis and staging of parotid lymph node metastasis in nasopharyngeal carcinoma: an analysis in 10,126 patients. Oral Oncol. 2019;95:150–6.

27. Guo SS, Liang YJ, Liu LT, Chen QY, Wen YF, Liu SL, Sun XS, Tang QN, Li XY, et al. Increased angiogenin expression correlates with Radiation Resistance and predicts poor survival for patients with nasopharyngeal carcinoma. Front Pharmacol. 2021;12:627935.

28. Hui EP, Li WF, Ma BB, Lam WKJ, Chan KCA, Mo F, Ai QYH, King AD, Wong CH, et al. Integrating postradiotherapy plasma Epstein-Barr virus DNA and TNM stage for risk stratification of nasopharyngeal carcinoma to adjuvant therapy. Ann Oncol. 2020;31:769–79.

29. Xue F, Ou D, Hu C, He X. Local regression and control of T1-2 nasopharyngeal carcinoma treated with intensity-modulated radiotherapy. Cancer Med. 2018;7:6010–9.

30. Wang G, He L, Yuan C, Huang Y, Liu Z, Liang C. Pretreatment MR imaging radiomics signatures for response prediction to induction chemotherapy in patients with nasopharyngeal carcinoma. Eur J Radiol. 2018;98:100–6.

31. Xiao-ping Y, Jing H, Fei-ping L, Yin H, Qiang L, Lanlan W, Wei W. Intravoxel incoherent motion MRI for predicting early response to induction chemotherapy and chemoradiotherapy in patients with nasopharyngeal carcinoma. J Magn Reson Imaging. 2016;43:1179–90.

32. Sun Z, Hu S, Xue Q, Jin L, Huang J, Dou W. Can 3D pseudo-continuous arterial spin labeling perfusion imaging be applied to predict early response to chemoradiotherapy in patients with advanced nasopharyngeal carcinoma? Radiother Oncol. 2021;160:97–106.

33. Shen H, Huang Y, Yuan X, Liu D, Tu C, Wang Y, Li X, Wang X, Chen Q, Zhang J. Using quantitative parameters derived from pretreatment dual-energy computed tomography to predict histopathologic features in head and neck squamous cell carcinoma. Quant Imaging Med Surg. 2022;12:1243–56.

34. Wu J, Lv Y, Wang N, Zhao Y, Zhang P, Liu Y, Chen A, Li J, Li X, et al. The value of single-source dual-energy CT imaging for discriminating microsatellite instability from microsatellite stability human colorectal cancer. Eur Radiol. 2019;29:3782–90.

35. Sato K, Morohashi H, Tsushima F, Sakamoto Y, Miura T, Fujita H, Umemura K, Suzuki T, Tsuruta S, et al. Dual energy CT is useful for the prediction of mesenteric and lateral pelvic lymph node metastasis in rectal cancer. Mol Clin Oncol. 2019;10:625–30.

36. Wang P, Tang Z, Xiao Z, Hong R, Wang R, Wang Y, Zhan Y. Dual-energy CT in differentiating benign sinonasal lesions from malignant ones: comparison with simulated single-energy CT, conventional MRI, and DWI. Eur Radiol. 2022;32:1095–105.

37. Lam S, Gupta R, Kelly H, Curtin HD, Forghani R. Multiparametric evaluation of Head and Neck squamous cell Carcinoma using a single-source dual-energy CT with fast kVp switching: state of the art. Cancers (Basel). 2015;7:2201–16.

38. Lv Y, Zhou J, Lv X, Tian L, He H, Liu Z, Wu Y, Han L, Sun M, et al. Dual-energy spectral CT quantitative parameters for the differentiation of Glioma recurrence from treatment-related changes: a preliminary study. BMC Med Imaging. 2020;20:5.

39. Roele ED, Timmer V, Vaassen LAA, van Kroonenburgh A, Postma AA. Dual-energy CT in Head and Neck Imaging. Curr Radiol Rep. 2017;5:19.

40. Forghani R, Kelly H, Yu E, Belair M, Letourneau-Guillon L, Le H, Proulx F, Ong T, Tan X, et al. Low-energy virtual monochromatic dual-energy computed tomography images for the evaluation of Head and Neck squamous cell carcinoma: a study of Tumor Visibility compared with single-energy computed tomography and user Acceptance. J Comput Assist Tomogr. 2017;41:565–71.

41. Zou Y, Zheng M, Qi Z, Guo Y, Ji X, Huang L, Gong Y, Lu X, Ma G, Xia S. Dual-energy computed tomography could reliably differentiate metastatic from non-metastatic lymph nodes of less than 0.5 cm in patients with papillary thyroid carcinoma. Quant Imaging Med Surg. 2021;11:1354–67.

42. Gao W, Zhang Y, Dou Y, Zhao L, Wu H, Yang Z, Liu A, Zhu L, Hao F. Association between extramural vascular invasion and iodine quantification using dual-energy computed tomography of rectal cancer: a preliminary study. Eur J Radiol. 2023;158:110618.

43. Yang L, Luo D, Yi J, Li L, Zhao Y, Lin M, Guo W, Hu L, Zhou C. Therapy effects of Advanced Hypopharyngeal and laryngeal squamous cell carcinoma: evaluated using dual-energy CT quantitative parameters. Sci Rep. 2018;8:9064.

44. Zhang G, Cao Y, Zhang J, Zhao Z, Zhang W, Zhou J. Epidermal growth factor receptor mutations in lung adenocarcinoma: associations between dual-energy spectral CT measurements and histologic results. J Cancer Res Clin Oncol. 2021;147:1169–78.

45. Zhao Y, Li X, Li L, Wang X, Lin M, Zhao X, Luo D, Li J. Preliminary study on the diagnostic value of single-source dual-energy CT in diagnosing cervical lymph node metastasis of thyroid carcinoma. J Thorac Dis. 2017;9:4758–66.

46. Qiu L, Hu J, Weng Z, Liu S, Jiang G, Cai X. A prospective study of dual-energy computed tomography for differentiating metastatic and non-metastatic lymph nodes of colorectal cancer. Quant Imaging Med Surg. 2021;11:3448–59.

47. Liu X, Ouyang D, Li H, Zhang R, Lv Y, Yang A, Xie C. Papillary thyroid cancer: dual-energy spectral CT quantitative parameters for preoperative diagnosis of metastasis to the cervical lymph nodes. Radiology. 2015;275:167–76.

Publisher's Note